ELSEVIER

Journal of Membrane Science 125 (1997) 123–142

journal of MEMBRANE SCIENCE

Limiting current density and water dissociation in bipolar membranes

H. Strathmann [a,*], J.J. Krol [a], H.-J. Rapp [b], G. Eigenberger [b]

[a] *University of Twente, Faculty of Chemical Technology, P.O. Box 217, 7500 AE Enschede, The Netherlands*
[b] *Universität Stuttgart, Institut für Chemische Verfahrenstechnik, Böblinger Straße 72, 70199 Stuttgart, Germany*

Received 9 January 1996; revised 20 May 1996; accepted 21 June 1996

Abstract

The behaviour of bipolar membranes in NaCl and Na_2SO_4 solutions is discussed. The membranes are characterized in terms of their limiting current densities. Below the limiting current density the electric current is carried by salt ions migrating from the transition region between the anion and the cation exchange layer of the bipolar membrane. In steady state these ions are replaced by salt ions transported from the bulk solutions into the transition region by diffusion and migration due to the fact that the ion-exchange layers are not strictly permselective. When the limiting current density is exceeded, the salt transport from the transition region can no longer be compensated by the transport into the region and a drastic increase in the membrane resistance and enhanced water dissociation is observed. This water dissociation is described as being a combination of the second Wien effect and the protonation and deprotonation of functional groups in the membrane. The limiting current density is calculated from a mass balance that includes all components involved in the transport. The parameters used in the mathematical treatment are the diffusion coefficients of salt ions and water, the ion mobilities in the membrane, the fixed charge densitiy of the membrane, the pK_b values of the functional groups and the solution bulk concentrations.

Keywords: Bipolar membrane; Membrane potentials; Limiting current density; Reaction layer

1. Introduction

The transport of ions across monopolar ion-exchange membranes can adequately be described by the Nernst–Planck equation [1–9]. With this equation and the assumption that electroneutrality in the system must be maintained membrane processes such as electrodialysis [10,11] can be described satisfactorily. However, many aspects of bipolar membranes, which resemble a laminate of a cation- and an anion-exchange layer are still subject of a rather controversial discussion. Especially the mechanism of the accelerated water dissociation and the location where exactly in the membrane it takes place is still not completely understood.

The work described in this paper is concentrated on elucidating the mechanism of the electrical potential enhanced water dissociation. Furthermore, the transport of ions through the bipolar membrane below the limiting current density is measured. Theo-

* Corresponding author.

PII S0376-7388(96)00185-8

retical considerations and calculated data are compared with measured current–voltage curves.

2. Fundamentals

2.1. The function of a bipolar membrane

Fig. 1 illustrates the structure and function of a bipolar membrane which consists of an anion and a cation selective layer joined together. By establishing an electric field across the membrane, charged species will be removed from the transition region between the two ion-exchange layers. When all salt ions are removed from the transition region, further transport of electric charges can be accomplished only by protons and hydroxyl ions that are available in very low concentrations, i.e. ca. 10^{-7} mol l^{-1} in completely demineralized water. The protons and hydroxyl ions removed from the transition region are replenished by the water dissociation equilibrium. The ability to generate protons and hydroxyl ions is used to produce or to recover acid and base from the corresponding salt solution [11–13].

2.2. Structure and thickness of the transition region

As far as the structure of the transition region between the two ion-exchange layers of a bipolar membrane is concerned two hypotheses exist. One postulates that the distance between the cation- and anion-exchange layer is zero and that the transition region is located within the two ion-exchange layers. Adjacent to the contacting surfaces of the two ion-exchange layers a region is obtained where the concentration of counter-ions is decreased and uncompensated fixed charges exist. This region is referred to as the "space charge region" [16] or "depletion layer" [17]. In correspondence to solid state physics nomenclature, the interphase in this case is called the "abrupt junction" [18]. The second hypothesis assumes a thin neutral region between the two ion-exchange layers [19]. This assumption leads to the so-called "neutral-layer model". The two models are illustrated in Fig. 2.

During operation of the membrane it can be assumed that almost all salt ions are removed from the transition region. The thickness 2λ can then be calculated from the electric resistance r_e^{tr} or the conductivity K^{tr} of the transition layer which is a function of the concentration c_j and the mobility u_j of the protons and hydroxyl ions. With

$$K^{tr} = F \sum_{j=1}^{n} z_j^2 c_j^{tr} u_j^{tr} \tag{1}$$

and

$$r_e^{tr} = \frac{2\lambda}{k^{tr}} \tag{2}$$

where F is the Faraday constant, z_j the valence of species j and r_e^{tr} the area multiplied resistance, the

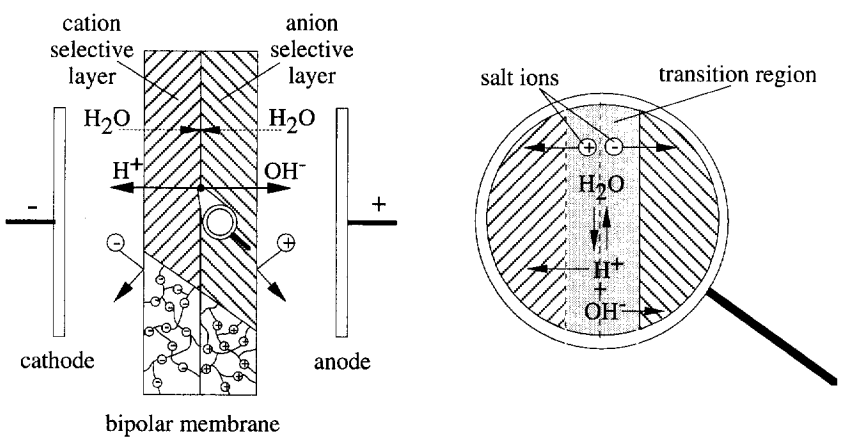

Fig. 1. Schematic drawing illustrating the function and structure of a bipolar membrane.

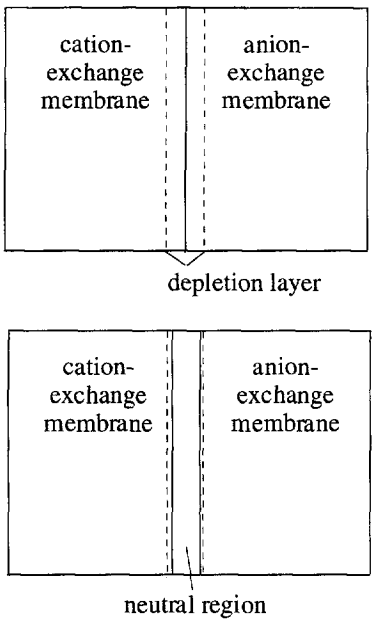

Fig. 2. Schematic drawing of two membrane models, i.e. the two-layer or abrupt junction model and the neutral-layer model.

thickness 2λ of the transition layer can be calculated according to:

$$2\lambda = r_e^{tr} F\left[\left(c_{H^+} u_{H^+}\right) + \left(c_{OH^-} u_{OH^-}\right)\right] \quad (3)$$

As a first approximation the electric resistance of a bipolar membrane r_e^{bm} can be considered as three resistances in series, i.e. the resistance of the cation-exchange membrane r_e^{cem}, the resistance of the transition region r_e^{tr} and that of the anion-exchange membrane r_e^{aem}:

$$r_e^{bm} = r_e^{cem} + r_e^{tr} + r_e^{aem} \quad (4)$$

The resistance of the transition region is thus given by:

$$r_e^{tr} = r_e^{bm} - \left(r_e^{cem} + r_e^{aem}\right) \quad (5)$$

The resistances of the cation- and anion-exchange membranes, r_e^{cem} and r_e^{aem}, respectively, are in the range of 0.5–5 Ωcm^2 [20–22,29]. The resistance of the bipolar membrane during the water dissociation is in the range of 10 Ωcm^2. By using an average value of 2.5 Ωcm^2 for the resistances of the monopolar layers, the calculated resistance of the transition region is 5 Ωcm^2. With $c_{H^+}^{tr} = c_{OH^-}^{tr} = 10^{-7}$ mol l^{-1} and the proton and hydroxyl ion mobilities taken from the literature [30], the calculated value for 2λ is ca. 2.7 nm.

From these theoretical considerations it can be estimated that the thickness of the transition region is in the range of a few nanometers. Fig. 3 shows a scanning electron micrograph of the junction be-

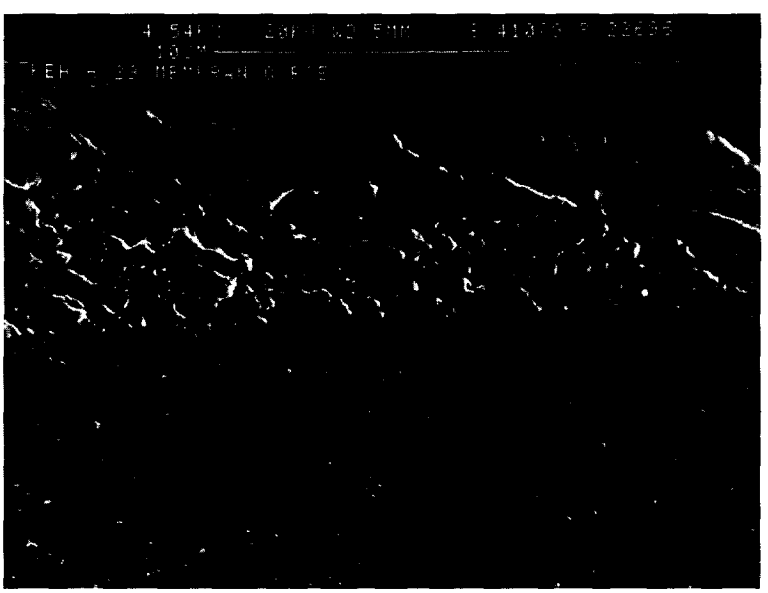

Fig. 3. Scanning electron micrograph of a bipolar membrane.

tween the monopolar layers of a commercial bipolar membrane. It can be seen that the thickness of the transition region is much smaller than 0.1 μm.

2.3. Concentration and potential profiles in bipolar membranes

The equilibrium between an ion-exchange membrane and the surrounding bulk solution can be described by the Donnan relation [23]. In 1962 Mauro [16] presented a continuum model describing the interphase between the membrane and the electrolyte. The model is based on an analogy between the p–n semi-conductor junction and the fixed charged membranes, i.e. the fixed charges in ion-exchange membranes play the same role as "doping" ions in semiconductors. By applying the Maxwell–Boltzmann and the Poisson equations to ion exchange membranes, concentration and potential profiles can be calculated.

The concentration of charged mobile species c_j in an electric field with an electrical potential of $\varphi(x)$ can be calculated by the Maxwell–Boltzmann relation:

$$c_j^{\varphi(x)} = c_j^{\varphi=0} e^{-zj\varphi(x)e_0/kT} \tag{6}$$

where e_0 and k are the elementary charge and the Boltzmann constant, respectively.

From Eq. (6) the Donnan potential φ_{Don} for ion-exchange membranes in equilibrium with a surrounding solution can be calculated. It is assumed that in the bulk phase, i.e. at a large distance from the membrane the potential $\varphi = 0$ and $c_j^{\varphi=0} = c_j^b$. In the membrane the potential is assumed to be $\varphi^m \neq 0$. With Eq. (6) this results in:

$$\frac{C_j^m}{c_j^b} = e^{-zj(\varphi^m - \varphi^b)e_0/kT} \tag{7}$$

The Donnan potential can then be calculated by:

$$\varphi_{Don} = \varphi^m - \varphi^b = \frac{1}{z_j} \ln \frac{c_j^b}{c_j^m} \frac{kT}{e_0} \tag{8}$$

Introducing the Avogadro number leads to:

$$\varphi_{Don} = \varphi^m - \varphi^b = \frac{RT}{z_j F} \ln \frac{c_j^b}{c_j^m} \tag{9}$$

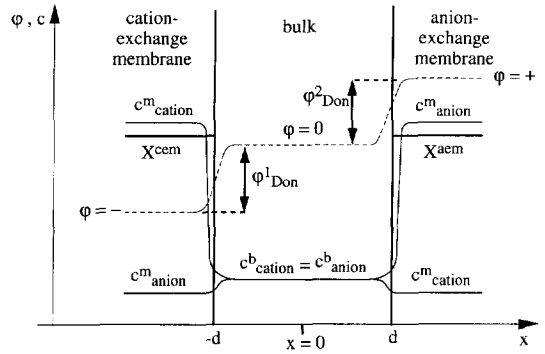

Fig. 4. Concentration and potential profiles for a cation- and an anion-exchange membrane separated by an electrolyte solution described by the Maxwell–Boltzmann equation.

It is further assumed that the electric potential satisfies the Poisson equation which is given by:

$$\frac{d^2\varphi}{dx^2} = -\frac{\rho_e}{\epsilon_0 \epsilon_r} \tag{10}$$

Here ϵ_0 is the permittivity of free space (vacuum) and ϵ_r the relative permittivity; ρ_e is the space charge density which can be calculated from:

$$\rho_e = \left(\sum_{j=1}^{n} z_j c_j + \sum_{l=1}^{n} \omega_l X_l \right) F \tag{11}$$

Here X_l is the fixed charge density and ω_l the electrochemical valence of the fixed charges.

The concentration and potential profiles of a cation- and anion-exchange membrane separated by an electrolyte solution are shown schematically in Fig. 4. The figure indicates that the electroneutrality at the interfaces is disturbed due to increasing or decreasing concentration of counter-ions and co-ions in the membranes and the bulk solution; there exists a so-called space charge region at the interfaces.

In the case of the abrupt junction, i.e. no neutral layer between the two ion-exchange layers, the space charge region is located completely within the membrane and uncompensated fixed charges exist in the region where anion- and cation-exchange layers meet as shown in Fig. 5.

For the symmetrical case, i.e. identical fixed charge densities in the cation- and anion-exchange

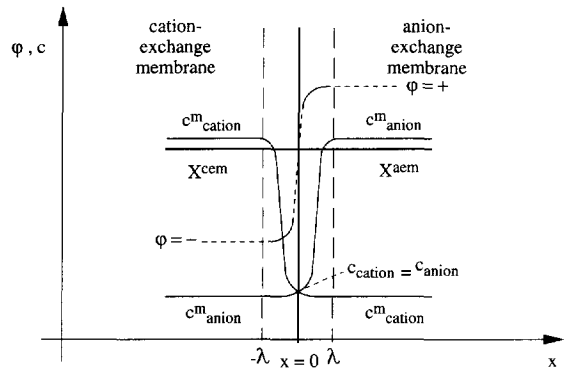

Fig. 5. Concentration and potential profiles for a bipolar membrane with an abrupt junction described by the Maxwell–Boltzmann equation.

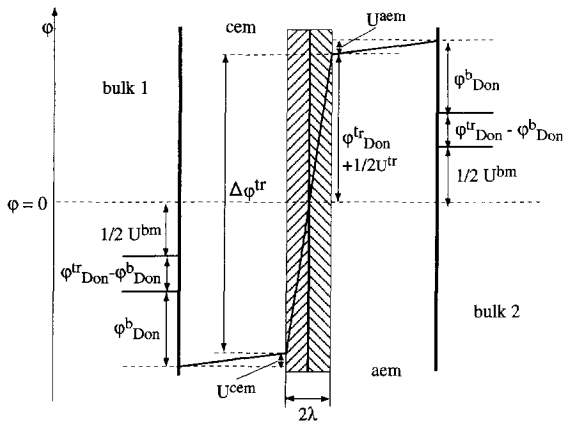

Fig. 6. Simplified potential profile across the bipolar membrane.

layers $X^{cem} = X^{aem} = X$, the thickness of the space charge or depletion layer can be calculated by [16]:

$$2\lambda = 2\sqrt{\frac{\Delta\varphi^{tr}\epsilon_0\epsilon_r}{XF}} \tag{12}$$

Here $\Delta\varphi^{tr}$ is the potential difference across the space charge layer which is given by:

$$\Delta\varphi^{tr} = 2|\varphi_{Don}| \tag{13}$$

If we assume that the system contains only monovalent ions and that $c^b \ll X$ is then:

$$c^m_{counter-ion} \approx X \tag{14}$$

and with

$$-\ln\frac{c^b_j}{X} = \ln\frac{x}{c^b_j} \tag{15}$$

the potential difference across the transition region $\Delta\varphi^{tr}$ can be determined to:

$$\Delta\varphi^{tr} = 2\left|\frac{RT}{z_jF}\ln\frac{c^b_j}{X}\right| = 2\frac{RT}{F}\ln\frac{X}{c^b_j} \tag{16}$$

With a fixed charge density $X = 1.0$ mol l^{-1} the calculated potential difference across the transition region at $T = 20°C$ (bipolar membrane in water $c^{tr}_{H^+} = c^{tr}_{OH^-} \approx 10^{-7}$ mol l^{-1}) is 0.814 V. The calculated thickness of the depletion layer (relative permittivity of water $\epsilon_r = 78.5$) according to Eqs. (12) and (16) is 4.84 nm.

Eq. (12) describes the thickness of the depletion layer if no external electrical field is applied. When an external voltage U^{bm} is established across the bipolar membrane the voltage drop across the depletion layer will be changed accordingly. Fig. 6 shows the simplified slope of the electric potential across the entire bipolar membrane when an external voltage U^{bm} is established and the diffusion potential of the monopolar membranes is neglected. For small current densities the voltage drop across the monopolar membranes U^{cem} and U^{aem} can also be neglected and $\Delta\varphi^{tr}$ can be described by:

$$\Delta\varphi^{tr} = 2|\varphi^{tr}_{Don}| + U^{bm} \tag{17}$$

In Eq. (17) U^{bm} is positive when the cation-exchange layer of the bipolar membrane is located on the cathode side as shown in Fig. 1 (reverse bias). The thickness of the transition region 2λ is then:

$$2\lambda = 2\sqrt{\frac{(2|\varphi^{tr}_{Don}| + U_{bm})\epsilon_{0_r}}{XF}} \tag{18}$$

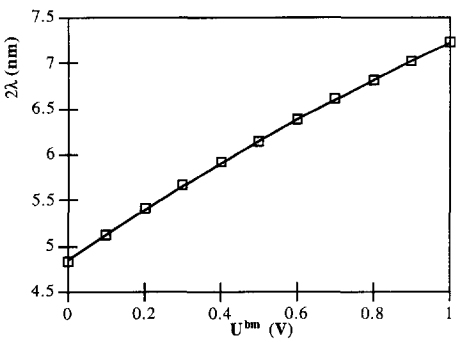

Fig. 7. Thickness 2λ of the transition region as a function of the applied voltage.

Eq. (18) shows that with increasing applied reverse bias the thickness of the depletion layer is increasing with the applied external voltage. This is demonstrated in Fig. 7 which shows the calculated increase of 2λ with increasing externally applied voltage U^{bm}.

3. Current–voltage relation and ion transport in bipolar membranes

3.1. Model for the transport of ions below the limiting current density

If we consider a bipolar membrane without external applied voltage, the concentration of mobile ions in the transition region is decreasing from the high counter-ion concentration to a small value which depends on the concentration in the bulk solutions as illustrated in Figs. 4 and 5. Due to the Donnan exclusion a potential difference is established across the transition region as described before. Diffusion of ions into this region caused by the concentration gradient $(\Delta c/\lambda)$ and migration of ions out of this area caused by the electric potential gradient $(\Delta\varphi^{tr}/2\lambda)$ are in equilibrium. This is valid for the abrupt junction as well as for the neutral layer model, so that for the following considerations the simplified concentration profiles illustrated in Fig. 8 are used. This figure shows the concentration profiles in a bipolar membrane and the adjacent bulk solutions of sodium chloride if no external voltage is applied.

If an external voltage U^{bm} is applied to the membrane, the equilibrium between concentration

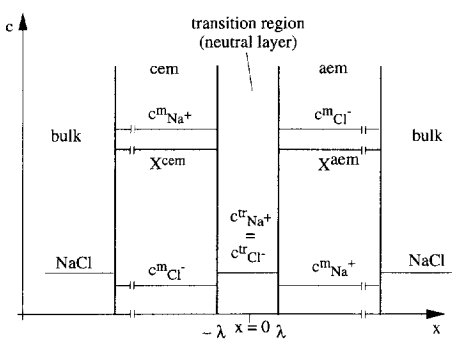

Fig. 8. Simplified concentration profiles of a bipolar membrane in a NaCl feed solution for $i \geq 0$.

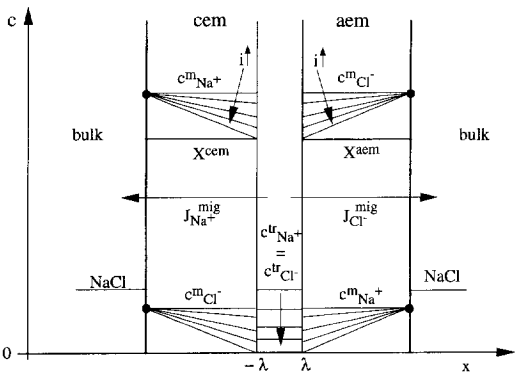

Fig. 9. Simplified concentration profiles of a bipolar membrane in a NaCl feed solution for $i \geq 0$.

gradient driving force and the electrical potential gradient driving force is disturbed and a net ion flux out of the transition region occurs. Thus, the transition region becomes depleted of salt ions as shown in Fig. 9 for a NaCl feed solution. At a certain current density, called the limiting current density i_{lim}, all salt ions are removed from the transition layer and the conductivity of this region can be calculated from the concentration of protons and hydroxyl ions which are available in completely deionized water in a concentration of 10^{-7} mol l^{-1}. The concentration of counter-ions in the monopolar membranes decreases in the direction of the junction and reaches the fixed charge density for $i = i_{lim}$ at $x = -\lambda$, λ.

Ion fluxes in a bipolar membrane in a NaCl feed solution for the conditions $0 < i < i_{lim}$ are illustrated in Fig. 10. In this case the following ion fluxes have to be considered:

1. Migration of counter-ions out of the transition region into the bulk solutions.
2. Migration of co-ions from the bulk solutions into the transition region.
3. Diffusion of co- and counter-ions from the bulk solutions into the transition region.

If the ion flux out of the bipolar membrane is higher than the ion flux into the membrane, the transition zone becomes depleted of salt ions, the resistance increases up to the resistance of deionized water, the electric field across this region increases and water dissociation takes place. Fig. 11 illustrates the diffusion of NaCl across the cation-exchange

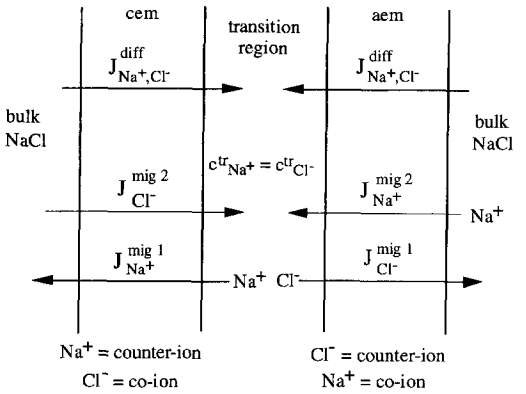

Fig. 10. Ion fluxes in a bipolar membrane in a NaCl solution for $0 < i < i_{lim}$ (reverse bias).

membrane. The ion concentrations at the interphases, $c^{mb}_{Na^+}$, $c^{mb}_{Cl^-}$, $c^{mtr}_{Na^+}$ and $c^{mtr}_{Cl^-}$, can be calculated from the Donnan equilibrium and the electroneutrality.

Due to the electroneutrality in the monopolar membranes, the diffusion of counter-ions (Na^+ in the cation-exchange membrane) is connected with the diffusion of co-ions (Cl^- in the cation-exchange membrane) and a common diffusion coefficient $D_{Na^+} = D_{Cl^-} = D_{NaCl}$ can be used. Diffusion coefficients of salts can be measured in a two compartment cell (1 mol l^{-1} NaCl||membrane||H_2O). The

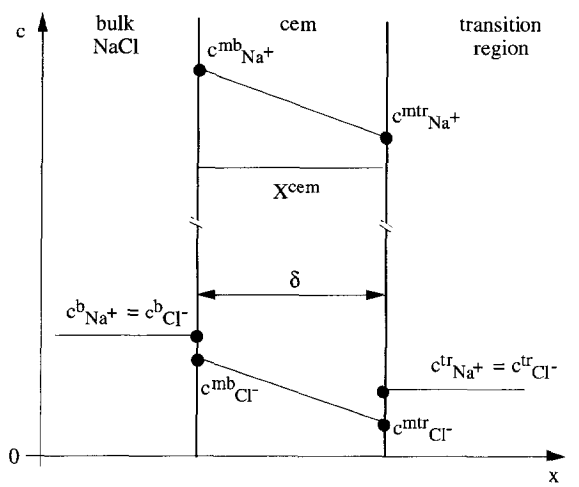

Fig. 11. Concentration profile across the cation-exchange membrane in a NaCl feed solution.

measured diffusion coefficients of NaCl across commercial cation-exchange membranes vary between 0.5×10^{-11} m^2 s^{-1} and 0.8×10^{-10} m^2 s^{-1}.

The limiting current density can be calculated for an 1–1 electrolyte (NaCl) with the following assumptions:

1. The thickness of the transition region is 3 nm.
2. All conditions are symmetrical. This means that the concentrations on both sides of the bipolar membrane are the same, that the monopolar layers have the same thickness $\delta = \delta^m$ and fixed charge density X, that the transport number of the sodium ions in the cation- exchange membrane $t^{cem}_{Na^+}$ equals the transport number of the chloride ions in the anion-exchange membrane $t^{aem}_{Cl^-}$, with $t^{cem}_{Na^+} = t^{aem}_{Cl^-} = t^*$ and that the monopolar layers have the same resistance r_e.
3. The concentration gradients of Na^+- and Cl^--ions across the monopolar layers show a linear relation.
4. Convection is neglected.
5. Transport of H^+ and OH^- is neglected ($c_{H^+} = c_{OH^-} = 10^{-7}$ mol l^{-1}).

Under these conditions the total voltage drop across the bipolar membrane U^{bm} can be calculated from the voltage drops across the different layers:

$$U^{bm} = U^{cem} + U^{tr} + U^{aem} = ir^{cem}_e + \frac{i2\lambda}{K^{tr}} + ir^{aem}_e \quad (19)$$

The conductivity of the transition region can be calculated according to Eq. (1). Since in the depletion region the sodium ion concentration is identical to that of the chloride ions $c^{tr}_{Na^+} = c^{tr}_{Cl^-}$ the change of the ion concentration in the transition zone can be determined from the flux of sodium ions, which is given by migration and diffusion through the cation- and anion-exchange:

$$V\frac{dc^{tr}_{Na^+}}{dt} = A\Sigma J_{Na^+} = A\left[J^{mig1}_{Na^+} + J^{mig2}_{Na^+} + 2J^{diff}_{Na^+}\right] \quad (20)$$

where $J^{diff}_{Na^+}$ is the diffusive sodium ion flux and $J^{mig1}_{Na^+}$ and $J^{mig2}_{Na^+}$ are the sodium ion migrations through the cation- and the anion-exchange membrane, respectively.

Since sodium is the counter-ion in the cation-exchange membrane and co-ion in the anion-exchange membrane, the migration of sodium ions is given by:

$$J_{Na^+}^{mig1} = -\frac{t_{Na^+}^{cem}}{zF} = -\frac{t^* i}{zF} \tag{21}$$

and

$$J_{Na^+}^{mig2} = \frac{t_{Na^+}^{aem} i}{zF} = \frac{(1 - t_{Cl^-}^{aem}) i}{zF} = \frac{(1 - t^*) i}{zF} \tag{22}$$

The sodium flux caused by diffusion is:

$$J_{Na^+}^{diff} = D_{NaCl} \frac{C_{Na^+}^{mb} - c_{Na^+}^{mtr}}{\delta^m} \tag{23}$$

Here D_{NaCl} is the diffusion coefficient of NaCl in the ion-exchange layers, δ_m is the thickness of the cation- and anion-exchange layer, respectively, t is the transport number, the superscripts cem and aem refer to cation- and anion-exchange membranes, respectively, and * refers to the transport number of a cation in a cation-exchange membrane or an anion in an anion-exchange membrane.

Under steady state conditions the concentration of sodium ions at the interphase between the transition region and membrane $c_{Na^+}^{mtr}$ can be calculated by combination of Eqs. (20) to (23):

$$c_{Na^+}^{mtr} = c_{Na^+}^{mb} - \frac{\delta^m i}{zF2D_{NaCl}}(t^* - (1 - t^*)) \tag{24}$$

The concentration of sodium ions at the membrane surface between the outer solution and membrane $c_{Na^+}^{mb}$ can be calculated from the Donnan equilibrium relation [23]:

$$\frac{c_{Na^+}^{b}}{c_{Na^+}^{mb}} = \frac{c_{Cl^-}^{mb}}{c_{Cl^-}^{b}} \tag{25}$$

Including the electroneutrality which is given by:

$$0 = \sum_{i=1}^{n} z_j c_j + \omega X \tag{26}$$

the concentration of the chloride ions at the membrane surface between the bulk phase and the membrane, $c_{Cl^-}^{mb}$ can be calculated in the case of the cation-exchange membrane, i.e. $\omega = -1$, by Eq. (26) to:

$$c_{Cl^-}^{mb} = -X + c_{Na^+}^{mb} \tag{27}$$

Introducing Eq. (27) into (25) with $c_{Na^+}^{b} = c_{Cl^-}^{b}$ results in:

$$\frac{c_{Na^+}^{b}}{c_{Na^+}^{mb}} = \frac{-X + c_{Na^+}^{mb}}{c_{Na^+}^{b}} \tag{28}$$

Rearranging Eq. (28) leads to:

$$c_{Na^+}^{mb} = \frac{X \pm \sqrt{X^2 + 4\left(c_{Na^+}^{b}\right)^2}}{2} \tag{29}$$

Introducing the positive solution of Eq. (29) into Eq. (27), $c_{Cl^-}^{mb}$ can be calculated.

The average concentration of sodium ions in the transition region agrees also with that obtained from the Donnan equilibrium. It can be calculated according to Eq. (28) where the bulk concentrations c_j^b are now replaced by the concentrations in the transition layer, c_j^{tr}:

$$c_{Na^+}^{tr} = \sqrt{\left(c_{Na^+}^{mtr}\right)^2 - X c_{Na^+}^{mtr}} \tag{30}$$

Introducing Eq. (29) into (24) leads to:

$$c_{Na^+}^{mtr} = \frac{X + \sqrt{X^2 + 4\left(c_{Na^+}^{b}\right)^2}}{2} - \frac{\delta^m i}{zF2D_{NaCl}}(t^* - (1 - t^*)) \tag{31}$$

Combination of Eqs. (30) and (31) results in:

$$c_{Na^+}^{tr} = \left[\left(\frac{X + \sqrt{X^2 + 4\left(c_{Na^+}^{b}\right)^2}}{2} - \frac{\delta^m i}{zF2D_{NaCl}}(t^* - (1 - t^*))\right)^2 - X\left(\frac{X + \sqrt{X^2 + 4\left(c_{Na^+}^{b}\right)^2}}{2} - \frac{\delta^m i}{zF2D_{NaCl}}(t^* - (1 - t^*))\right)\right]^{1/2} \tag{32}$$

From these equations the limiting current density can be calculated with $c_{Na^+}^{tr} = 0$, i.e. the condition at which the limiting current density is reached.

Fig. 12 shows the calculated current–voltage curve up to the limiting current density for the following parameters: $\delta^m = 100$ μm, $c^b_{Na^+} = 0.5$ mol l^{-1}, $r_e = 2.5$ Ωcm^2, $t^* = 0.99$, $2\lambda = 3$ nm, $X = 1.5$ mol l^{-1}, $D_{NaCl} = 7.0 \times 10^{-11}$ m^2 s^{-1}.

The presented model describes the current–voltage behaviour up to the point where the limiting current density is reached. For the conditions used in Fig. 12 the limiting current density is $i = i_{lim} = 2.09$ mA cm^{-2}. At this point all salt ions are removed from the transition region and the resistance of the membrane increases drastically. When the limiting current density is exceeded water dissociation starts in the bipolar membrane.

3.2. Measured and calculated current voltage curves of bipolar membranes

The current–voltage curves of bipolar membranes have been determined in a six-compartment cell which is described in detail elsewhere [14]. The voltage drop across the membrane is measured by Haber–Luggin capillaries placed directly on both surfaces of the bipolar membrane. The potential difference between the two capillaries is measured as a function of the electric current passing through the membrane.

Three different commercially available membranes were tested. The first membrane, referred to as bm1 was supplied by Tokuyama Soda Corporation, Japan. The membrane has an integral structure and is reinforced. It had the appearance and handling

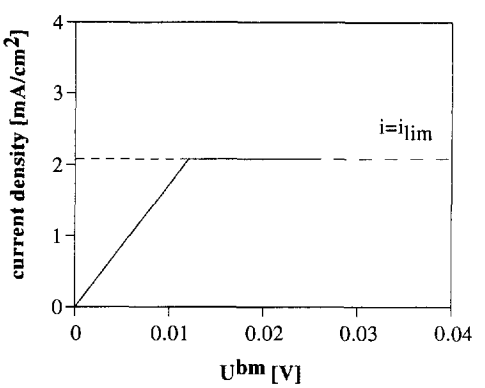

Fig. 12. Calculated current–voltage curve of a bipolar membrane up to the limiting current density.

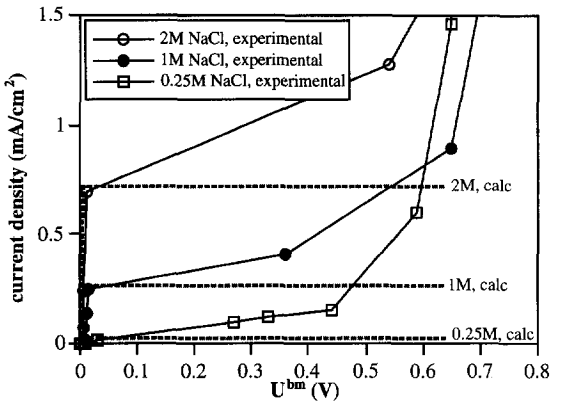

Fig. 13. Comparison between measured and calculated limiting current densities for bipolar membrane bm1 (parameters used in the calculations: $\delta^m = 100$ μm, $2\lambda = 3$ nm, $X = 1.5$ mol l^{-1}, $D_{NaCl} = 2.59 \times 10^{-12}$ m^2 s^{-1}, $t^* = 0.99$, $r_e = 2.5$ Ω cm^2).

capability of a normal ion-exchange membrane. The second membrane, referred to as bm2, was supplied by WSI Technologies Inc., USA. The membrane was a composite of two separate non-reinforced sheets and significantly thinner than regular ion-exchange membranes. The third membrane, bm3, was supplied by Fumatech GmbH, Germany. The membrane was an integral reinforced structure and its appearance and handling properties were that of a regular ion-exchange membrane.

First current–voltage curves were measured with the bipolar membrane bm1 and sodium chloride solutions of various concentrations and compared with calculated data. Fig. 13 shows the measured and calculated data. The solid lines represent the measured data and the dotted lines indicate the calculated limiting current densities. It should be pointed out that the calculation of the current/voltage curves and the limiting current densities by Eq. (32) are based on the assumption that the current through the bipolar membrane is carried by salt ions only. Thus, when the limiting current density is reached, the interphase between the cation and anion exchange layers will be depleted of salt ions and an increase in the applied voltage should not lead to an increase in current. In reality however, this assumption is not valid since in the interphase between the cation- and anion-exchange layer of the bipolar membrane H^+- and OH^--ions will be generated due to an electric field enhanced water dissociation and with increas-

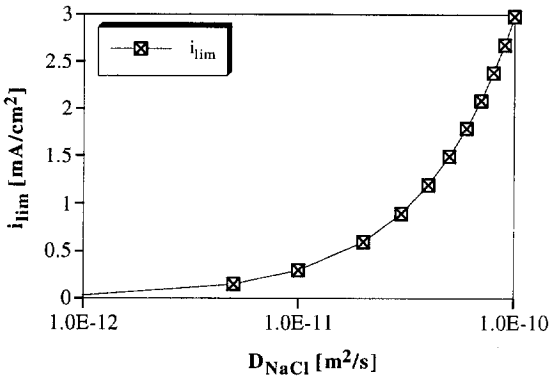

Fig. 14. Calculated influence of the diffusion coefficient D_{NaCl} on the limiting current density i_{lim} ($X = 1.5$ mol l^{-1}, $c^{b}_{Na^+} = 0.5$ mol l^{-1}, $t^* = 0.99$).

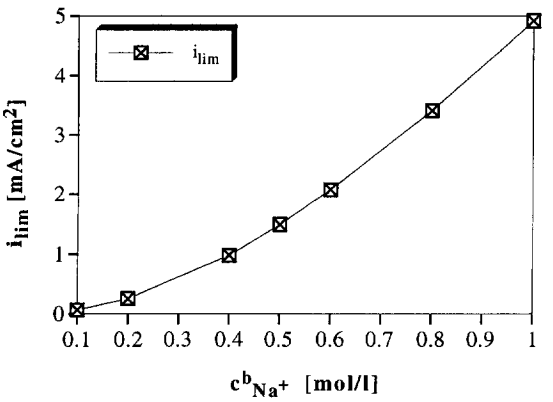

Fig. 15. Calculated influence of the bulk concentration $c^{b}_{Na^+}$ on the limiting current density ($X = 1.5$ mol l^{-1}, $D_{NaCl} = 5.0 \times 10^{-11}$ m^2 s^{-1}, $t^* = 0.99$).

ing applied voltage the current will increase due to the generation of protons and hydroxyl ions. The actual mechanism of this electric field enhanced water dissociation is discussed in the second part of this paper. Thus, the dotted curves in Fig. 13 indicate the maximum current density achievable without considering electric field enhanced water dissociation.

From Eqs. (20) and (32) it can be seen that the limiting current density depends on the diffusion and the migration of ions into the membrane. The diffusion furthermore depends on the diffusion coefficient of NaCl in the membrane, the thickness δ^m of the monopolar layers and the concentration of ions in the membrane $c^{mb}_{Na^+}$ which is a function of the bulk concentration $c^{b}_{Na^+}$ and the fixed charge density X. The migration of co-ions into the membrane depends on the transport number t^*. The relation between the limiting current density and the diffusion coefficient of NaCl in the membrane is shown in Fig. 14 where the limiting current densities of bipolar membranes are calculated according to Eq. (32) as a function of the diffusion coefficient of sodium chloride D^{m}_{NaCl}. Fig. 15 shows calculated limiting current densities as a function of the bulk solution concentration $c^{b}_{Na^+}$. The limiting current density as a function of the fixed charge density X is shown in Fig. 16.

It is clear that by increasing the diffusion coefficient D^{m}_{NaCl} the back-diffusion of ions into the transition region and thus the limiting current density i_{lim} is increasing. Increasing bulk concentration $c^{b}_{Na^+}$ has the same effect as also indicated by the experimental results shown in Fig. 13. By increasing the fixed charge density X the Donnan exclusion is improved and thus i_{lim} decreases.

Current–voltage curves were also measured with the bipolar membranes bm2 and bm3 in a 0.25 mol l^{-1} Na_2SO_4 solution at current densities below the limiting current density. The results are shown in Fig. 17. When comparing Figs. 13 and 17 it can be seen that different bipolar membranes can have rather different limiting current densities. Bipolar membrane bm2 is a very thin and highly permeable membrane and has a significantly higher limiting current density than the two other bipolar membranes due to its higher salt diffusivity.

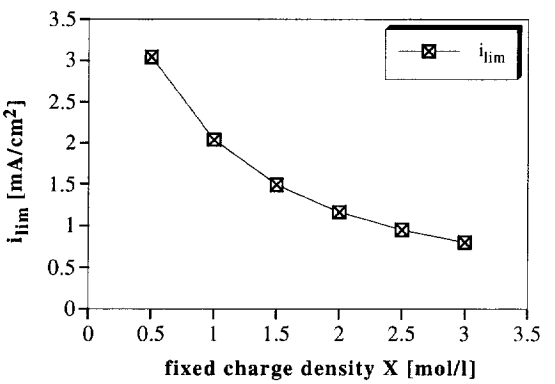

Fig. 16. Calculated influence of the fixed charge density on the limiting current density ($t^* = 0.99$, $D_{NaCl} = 5.0 \times 10^{-11}$ m^2 s^{-1}, $c^{b}_{Na^+} = 0.5$ mol l^{-1}).

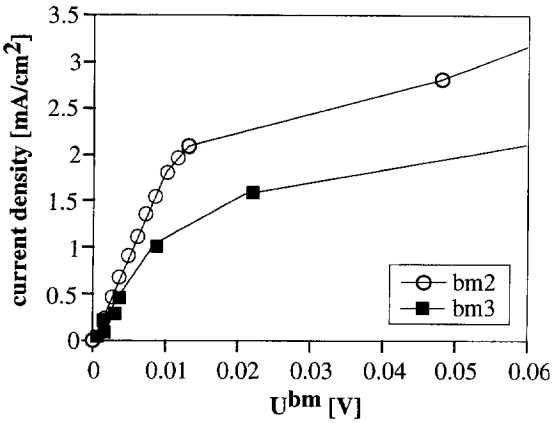

Fig. 17. Limiting current densities for bipolar membranes bm2 and bm3 determined in a 0.25 mol l^{-1} Na_2SO_4 solution.

Current–voltage curves were also measured at current densities much higher than the limiting current density. The results are depicted in Fig. 18 which shows the current–voltage relation of the three different bipolar membranes in a 0.25 molar Na_2SO_4 bulk solution up to current densities of 100 mA cm^{-2}. At low current densities the resistance is more or less constant until the so-called limiting current density is reached. Then the resistance increases drastically and the current is hardly increased with increasing applied voltage until a certain voltage drop across the membrane is reached. At this point the resistance decreases sharply and the current density increases with only a slightly increased voltage drop. Although the current–voltage curves of the three membranes are different (the membrane with

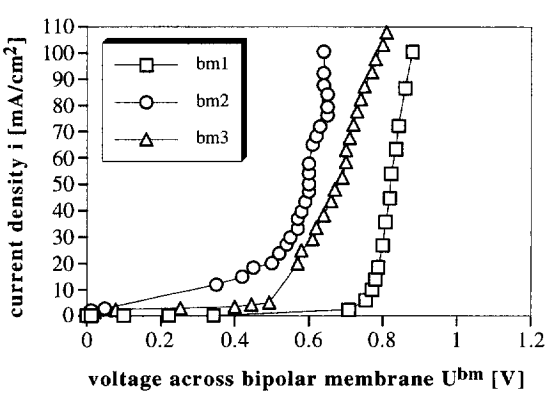

Fig. 18. Measured current–voltage curves of three different bipolar membranes in 0.25 mol l^{-1} Na_2SO_4 at high current densities.

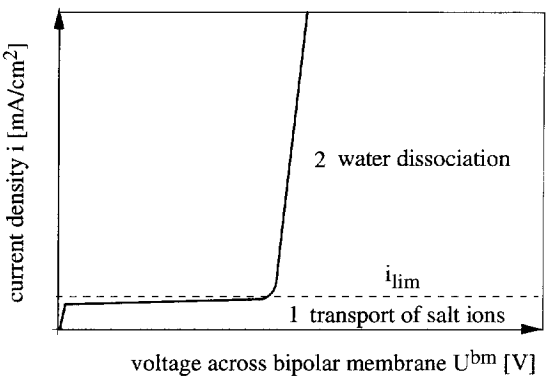

Fig. 19. Schematical current–voltage curve of bipolar membranes.

the highest salt permeability shows the lowest electrical resistance) the curves follow a general trend. This typical behaviour of bipolar membranes is schematically shown in Fig. 19. Similar current–voltage curves are reported in the literature [14,15]. The sharp increase in the current density when a certain value of the applied external voltage is exceeded is generally attributed to the onset of an electric field enhanced water dissociation.

While the current–voltage behaviour of bipolar membranes at current densities below the limiting current densities can satisfactorily be rationalized with the arguments described by Eq. (32) of this paper it is significantly more difficult to rationalize the water dissociation mechanism that leads to the drastic increase in current density when a certain voltage is exceeded.

4. The mechanism of the water dissociation

4.1. Accelerated water splitting in bipolar membranes

The water dissociation equilibrium is given by:

$$2H_2O \underset{k_{-1}}{\overset{k_1}{\Leftrightarrow}} H_3O^+ + OH^- \qquad (a)$$

Assuming that the water dissociation in a bipolar membrane takes place by reaction (a) the maximum current carried by H^+ and OH^- can be calculated from:

$$i = Fk_1 c^{tr}_{H_2O} 2\lambda \qquad (33)$$

Assuming a thickness of the transition layer of $2\lambda = 3$ nm, a water concentration in the transition layer of $c^{tr}_{H_2O} = 6$ mol l^{-1} [20] and a water dissociation rate constant of $k_1 = 2 \times 10^{-5}$ s^{-1} the maximum current that can be obtained from the water dissociation according to reaction (a) is 3.5×10^{-5} A m^{-2}. From experiments with bipolar membranes we know that current densities of more than 2000 A m^{-2} are possible. This means that there must be an effect which accelerates the water dissociation in bipolar membranes about 5×10^7 times.

4.2. The second Wien effect

The first attempt to explain the enhanced water dissociation in bipolar membranes was based on the so-called second Wien effect which describes the influence of a strong electric field on the water dissociation constant k_1 while the recombination rate constant k_{-1} is not effected by the electric field. According to the second Wien effect, which is discussed in detail in [28], the ratio of the dissociation rate constant under the influence of an electric field, $k_{d(E)}$, to that without an electrical field, k_d, can be determined by:

$$\frac{k_{d(E)}}{k_d} = 1 + b + \frac{b^2}{3} + \frac{b^3}{18} + \frac{b^4}{180} + \frac{b^5}{2700} + \frac{b^6}{56700} + \ldots \quad (34)$$

with

$$b = 0.09636 \frac{E}{\epsilon_r T^2} \quad (35)$$

Here E is the electric field density and ϵ_r the relative permittivity.

In Eq. 35 the electric field density E has to be inserted in V m^{-1}. The relative permittivity ϵ_r depends on the electrolyte and is 78.57 at 25°C in water [29]. In the case of high field intensities ($E > 10^8$ V m^{-1}) Eq. (36) can be used to calculate the effect of the electric field on the dissociation rate constant:

$$\frac{k_{d(E)}}{k_d} = \left(\frac{2}{\pi}\right)^{1/2} (8b)^{-3/4} e^{(8b)^{1/2}} \quad (36)$$

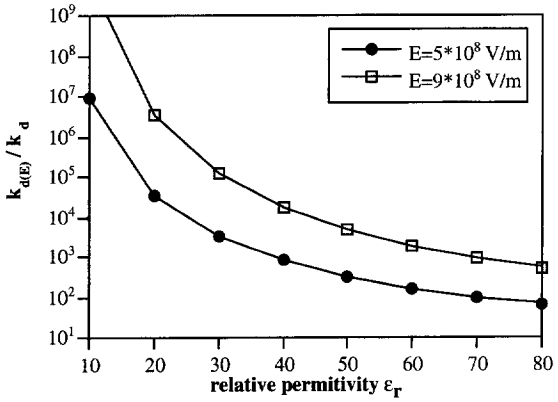

Fig. 20. $k_{d(E)} / k_d$ calculated from the second Wien effect.

Since the thickness of the transition zone is in the range of 6 nm when U^{bm} is one Volt (see Fig. 7), the electric field intensity ($E = \Delta\varphi^{tr}/2\lambda$) is in the range of 6.0×10^8–9.0×10^8 V m^{-1}. Fig. 20 shows the calculated increase of the water dissociation rate constant due to an electric field density of $E = 5.0 \times 10^8$ V m^{-1} and $E = 9.0 \times 10^8$ V m^{-1} as a function of ϵ_r. From Fig. 20 it can be seen that the second Wien effect can explain the enhanced water dissociation only if ϵ_r is smaller than 10. Furthermore, if the accelerated water dissociation would only be due to the second Wien effect, it should be identical for both anion- and cation-exchange membranes, but this is not the case [24].

4.3. Influence of the charged groups in ion-exchange membranes on the water dissociation rate

Water dissociation was first observed in electrodialysis when the limiting current density was exceeded. It was shown that the water dissociation occurred mainly at the anion and not at the cation-exchange membrane [24]. This indicates that the water splitting does not take place in the solution but in the membrane phase. Based on these general observations Simons [25–27] suggested that with anion-exchange membranes the water dissociation is caused by a reversible protonation of weakly basic groups, i.e. tertiary amines. He further showed: (1) that water splitting can be eliminated by methylation of the tertiary amines resulting in quaternary amines, (2) that degradation of quaternary ammonium groups

in strongly basic environment leads to tertiary amines [25] and (3) that water splitting at cation exchange membranes can be obtained only when weak acids (proline, phenol) are present in the solution next to the membrane surface, or when the membrane contains weakly acidic groups, such as carboxylic acid. Following the reasoning of Simons, water dissociation in membranes can take place by the following reactions:

$$B + H_2O \underset{k_{-2}}{\overset{k_2}{\Leftrightarrow}} BH^+ + OH^- \quad (b)$$

$$BH^+ + H_2O \underset{k_{-3}}{\overset{k_3}{\Leftrightarrow}} B + H_3O \quad (c)$$

and

$$A^- + H_2O \underset{k_{-4}}{\overset{k_4}{\Leftrightarrow}} AH + OH^- \quad (d)$$

$$AH + H_2O \underset{k_{-5}}{\overset{k_5}{\Leftrightarrow}} A^- + H_3O^+ \quad (e)$$

where B is a neutral base and AH a neutral acid.

4.4. Model for the water dissociation in bipolar membranes

The present model is developed under the following assumptions:

- Water dissociation occurs in the depletion anion-exchange layer of the membrane.
- Water dissociation is accelerated by protonation and deprotonation of weakly basic groups.
- The water dissociation is also accelerated by the electric field according to the second Wien effect, which increases k_1 (reaction (a)), k_2 and k_3 (reactions (b) and (c)).
- The voltage drop across the ion-exchange layers of the bipolar membrane U^{cem} and U^{aem} are neglected so that $U^{tr} = U^{bm}$.
- The generated protons and hydroxyl ions are removed from the transition region by migration and the electric current is calculated from this migration flux.
- The driving force for the migration of protons and hydroxyl ions $d\varphi/dx$ is $U^{tr}/2\lambda$, since $2 \times \varphi^{tr}_{Don}$ is in equilibrium with the diffusion of ions into the transition region.

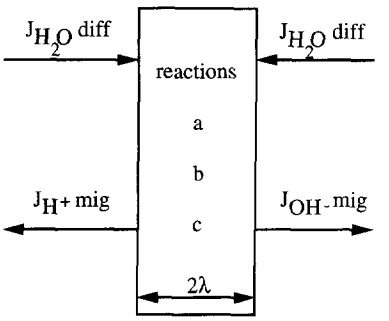

Fig. 21. Simplified system for the mass balance.

- Water is transported into the transition region by diffusion.

For each species j of our simplified system which is illustrated in Fig. 21, the following mass balance is valid:

$$2\lambda \frac{dc_j^{tr}}{dt} = \left(J_j^{diff} + J_j^{mig}\right) + 2\lambda r_j \quad (37)$$

Here r_j are the reaction rates of the different components in the transition layer, i.e. the protons and hydroxyl ions and the protonated and the neutral base.

The reaction rates r_j are:

$$r_{H_3O^+} = k_1 c_{H_2O} - k_{-1} c_{H_3O^+} c_{OH^-} + k_3 c_{BH^+} c_{H_2O} - k_{-3} c_{H_3O^+} c_B \quad (38)$$

$$r_{OH^-} = k_1 c_{H_2O} c_{H_2O} - k_{-1} c_{H_3O} c_{OH^-} + k_2 c_B c_{H_2O} - k_{-2} c_{BH^+} c_{OH^-} \quad (39)$$

$$r_B = k_3 c_{BH^+} c_{H_2O} - k_{-3} c_{H_3O^+} c_B + k_{-2} c_{BH^+} c_{OH^-} - k_2 c_B c_{H_2O} \quad (40)$$

$$r_{BH^+} = -r_B = -k_3 c_{BH^+} c_{H_2O} + k_{-3} c_{H_3O^+} c_B - k_{-2} c_{BH^+} c_{OH^-} + k_2 c_B c_{H_2O} \quad (41)$$

and

$$r_{H_2O} = k_{-1} c_{H_3O^+} c_{OH^-} - k_1 c_{H_2O} c_{H_2O} + k_{-2} c_{BH^+} c_{OH^-} - k_2 c_B c_{H_2O} + k_{-3} c_{H_3O^+} c_B - k_3 c_{BH^+} c_{H_2O} \quad (42)$$

In case of reaction (a) there is

$$r_1 = k_1 [H_2O][H_2O] = k_1' [H_2O] \quad (43)$$

$$r_{-1} = k_{-1} [H_3O^+][OH^-] \quad (44)$$

In equilibrium the reaction rates r_1 and r_{-1} are identical and combination of Eqs. (43) and (44) leads to:

$$\frac{k'_1}{k_{-1}} = \frac{[H_3O^+][OH^-]}{[H_2O]} = \frac{K_w}{[H_2O]} = \frac{K_w}{55\,\text{mol/l}} \tag{45}$$

With $K_w = 10^{-14}$ mol^2 l^{-2} and $k'_1 = 2 \times 10^{-5}$ s^{-1} [19] k_{-1} is calculated from Eq. (45) to be 1.1×10^{11} l mol^{-1} s^{-1}.

Furthermore, k_1 can be calculated from Eq. (43) to be 3.63×10^{-7} l mol^{-1} s^{-1}.

In case of reaction (b) is:

$$\frac{[BH^+][OH^-]}{[B]} = K_b = \frac{k'_2}{k_{-2}} \tag{46}$$

or

$$k'_2 = k_{-2} K_b = k_{-2} \times 10^{-pK_b} \tag{47}$$

Here $pK_b = -\log K_b$

In case of reaction (c) is:

$$\frac{[B][H_3O^+]}{[BH^+]} = K_a = \frac{k'_3}{k_{-3}} \tag{48}$$

or

$$k'_3 = k_{-3} K_a = k_{-3} \times 10^{-pK_a} \tag{49}$$

With $pK_a + pK_b = 14$ Eq. (49) becomes:

$$k'_3 = k_{-3} \times 10^{-(14-pK_b)} \tag{50}$$

Furthermore, k_2 and k_3 can be calculated from the following relations:

$$k_2 = \frac{k'_2}{[H_2O]} = \frac{k_{-2} \times 10^{-pK_b}}{[H_2O]} \tag{51}$$

and

$$k_3 = \frac{k'_3}{[H_2O]} = \frac{k_{-3} \times 10^{-(14-pK_b)}}{[H_2O]} \tag{52}$$

From the literature it is known that the rate constants k_{-2} and k_{-3} in aqueous solutions are in the range of 10^{10}–10^{11} l mol^{-1} s^{-1} [19] and that they are not influenced by the electric field. Furthermore, it is assumed that k_{-2} and k_{-3} are 10^{11} l mol^{-1} s^{-1} (k_{-1} was calculated to be 1.1×10^{11} l mol^{-1} s^{-1}).

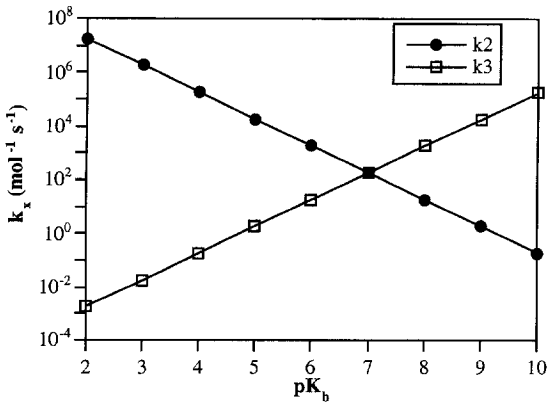

Fig. 22. Influence of the basicity of the membrane groups on the dissociation rate constant.

Fig. 22 shows the calculated values of k_2 and k_3 as a function of the pK_b-value. It can be seen that for strongly basic groups ($pK_b < 1$) k_2 is very high and k_3 is very small. This means that the protonation is very fast but the deprotonation is very slow, so that the groups remain in the protonated form. For strongly acidic groups $pK_a < 0$ all groups remain in the dissociated, deprotonated form. With decreasing basicity of the groups (increasing pK_b) k_2 is decreasing while k_3 is increasing. At $pK_b = 7$ the deprotonation is as fast as the protonation and $k_2 = k_3 = 180 = 49.6 \times 10^7 \times k_1$. This demonstrates that the proton transfer reactions are capable of explaining the enhanced water dissociation.

Within the model the diffusional water transport into the membrane is described by Ficks law:

$$J^{\text{Diff}}_{H_2O} = -D_{H_2O} \frac{dc_{H_2O}}{dx} \approx D_{H_2O} \frac{c^{\text{mb}}_{H_2O} - c^{\text{tr}}_{H_2O}}{\delta} \tag{53}$$

The water concentration gradient in the membrane is assumed to be linear as shown in Fig. 23 and the migration of protons and hydroxyl ions is calculated with the Nernst–Plank equation:

$$J^{\text{mig}}_{H^+} = u^{\text{tr}}_{H^+} c^{\text{tr}}_{H^+} \frac{U^{\text{tr}}}{2\lambda} \tag{54}$$

and

$$J^{\text{mig}}_{OH^-} = u^{\text{tr}}_{OH^-} c^{\text{tr}}_{OH^-} \frac{U^{\text{tr}}}{2\lambda} \tag{55}$$

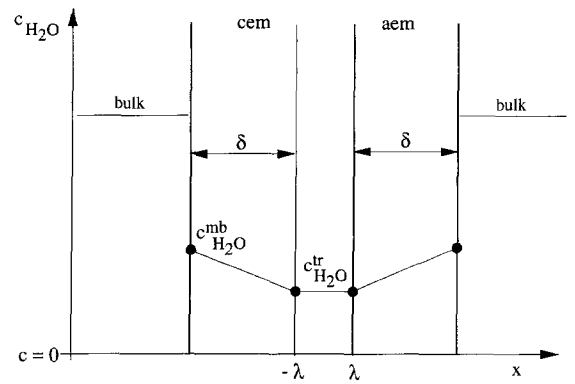

Fig. 23. Profile of the water concentration in the membrane.

Introducing the derived relations into Eq. (37) the change in the concentrations of the different species in the transition region can be calculated by:

$$\frac{dc^{tr}_{H_3O^+}}{dt} = k_1 c_{H_2O} c_{H_2O} - k_{-1} c_{H_3O^+} c_{OH^-} + k_3 c_{BH^+} c_{H_2O} - k_{-3} c_{H_3O^+} c_B - \frac{u_{H^+} c_{H^+}}{2\lambda} \frac{U^{tr}}{2\lambda} \quad (56)$$

$$\frac{dc^{tr}_{OH^-}}{dt} = k_1 c_{H_2O} c_{H_2O} - k_{-1} c_{H_3O^+} c_{OH^-} + k_2 c_B c_{H_2O} - k_{-2} c_{BH^+} c_{OH^-} - \frac{u_{OH^-} c_{OH^-}}{2\lambda} \frac{U^{tr}}{2\lambda} \quad (57)$$

$$\frac{dc^{tr}_B}{dt} = k_3 c_{BH^+} c_{H_2O} - k_{-3} c_{H_3O^+} c_B + k_{-2} c_{BH^+} c_{OH^-} - k_2 c_B c_{H_2O} \quad (58)$$

$$\frac{dc^{tr}_{BH^+}}{dt} = -\frac{dc^{tr}_B}{dt} \quad (59)$$

and

$$\frac{dc^{tr}_{H_2O}}{dt} = k_{-1} c_{H_3O^+} c_{OH^-} - k_1 c_{H_2O} + k_{-2} c_{BH^+} c_{OH^-} - k_2 c_B c_{H_2O} + k_{-3} c_{H_3O^+} c_B - k_3 c_{BH^+} c_{H_2O} + 2\frac{D_{H_2O}}{2\lambda} \frac{c^{mb}_{H_2O} - c^{mtr}_{H_2O}}{\delta} \quad (60)$$

The electric current can be calculated from the hydroxyl ion flux as follows:

$$I = FA \sum_{i=1}^{n} z_j J_j = FA u^{tr}_{OH^-} c^{tr}_{OH^-} \frac{U^{tr}}{2\lambda} \quad (61)$$

or

$$i = \frac{I}{A} = F u^{tr}_{OH^-} c^{tr}_{OH^-} \frac{U^{tr}}{2\lambda} \quad (62)$$

Because of their higher mobility the protons will first move faster than the hydroxyl ions. This disturbs the electroneutrality and leads to an additional electric field which increases the migration of the hydroxyl ions and slows down the protons. To take this phenomenon into account both mobilities are assumed to be $u_{H^+} = u_{OH^-} = 30.0 \times 10^{-8}$ m^2 V^{-1} s^{-1}.

4.5. Results from the model calculations

To determine the steady state of the described system, the five differential Eqs. (56)–(60) were solved as a function of time by using the parameters listed in Table 1.

Fig. 24 shows the protonation and deprotonation of basic groups B as a function of time. At first all groups are assumed to be in the deprotonated form. With increasing time the number of protonated groups $c^{tr}_{BH^+}$ is increasing while c_B is decreasing. At 10^{-4} s

Table 1
Concentrations at time $t \approx 0$, i.e. the beginning of the calculation and other parameters used for the determination of the steady state

Parameter	Value
$c^{tr,0}_B$	1000 mol m^{-3}
c^b	100 mol m^{-3}
$c^{bm}_{H_2O}$	6000 mol m^{-3}
$c^{tr,0}_{H_2O}$	6000 mol m^{-3}
$c^{tr,0}_{H^+}$	10^{-4} mol m^{-3}
$c^{tr,0}_{OH^-}$	10^{-4} mol m^{-3}
D_{H_2O}	10^{-9} m^2 s^{-1}
δ	80 μm
k_1	3.36×10^{-10} m^3 mol^{-1} s^{-1}
k_{-1}	1.1×10^{8} m^3 mol^{-1} s^{-1}
k_{-2}	1.0×10^{8} m^3 mol^{-1} s^{-1}
k_{-3}	1.0×10^{8} m^3 mol^{-1} s^{-1}

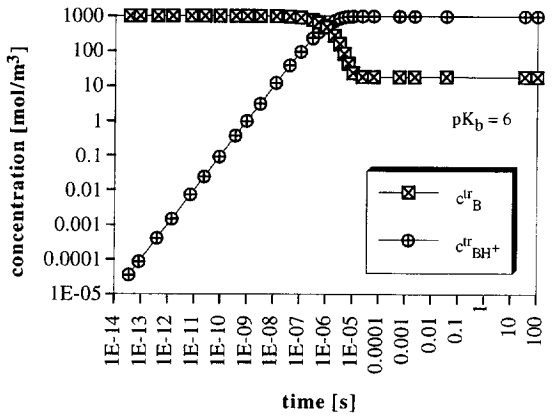

Fig. 24. Protonation of basic groups B as a function of time.

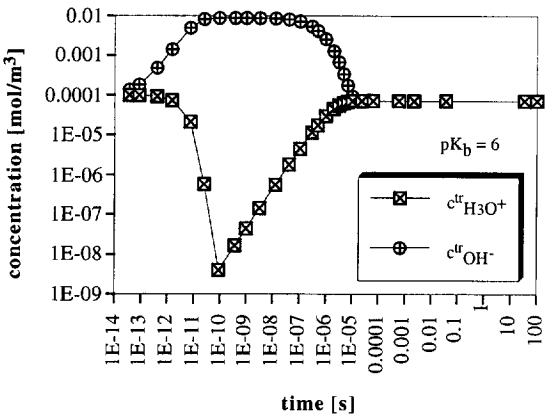

Fig. 25. Concentration of H_3O^+ and OH^- as a function of time.

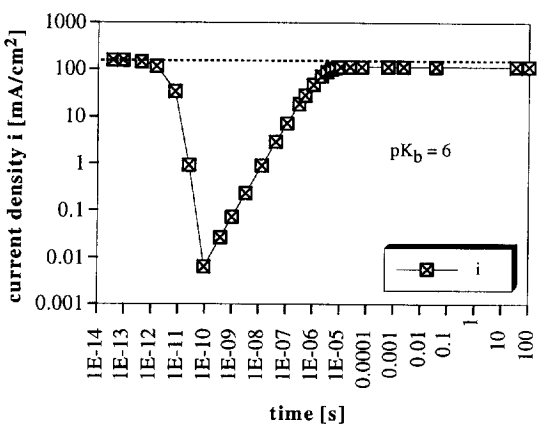

Fig. 26. Current density i as a function of time.

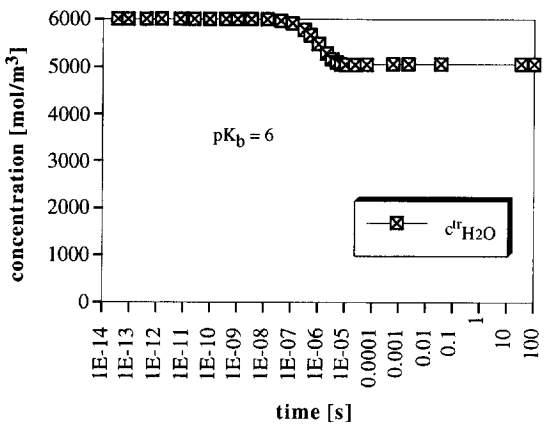

Fig. 27. Water concentration in the transition region as a function of time.

the steady state is reached with $c^{tr}_{BH^+} = 982$ and $c_B = 18$ mol m^{-3}.

Because of the rapidly increasing concentration of protonated groups BH^+, the concentration of protons is decreasing and the concentration of hydroxyl ions is increasing as shown in Fig. 25. For a short time of about 10^{-5} s the electroneutrality is disturbed, while in the steady state $c_{H_3O^+}$ equals c_{OH^-} due to the assumed equal mobility of H^+ and OH^-.

The calculated current density is shown in Fig. 26. Fig. 27 illustrates the decreasing water concentration in the transition region due to the consumption of water by the water dissociation. In Figs. 28–31 the calculated current–voltage curves due to the water dissociation in the steady state ($t > 100$ s) are shown. For this calculation the parameters listed in Table 1 are used. Fig. 28 illustrates the influence of

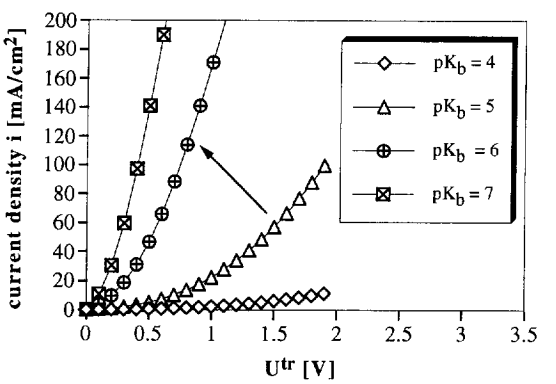

Fig. 28. Influence of the pK_b-value on the current–voltage curve.

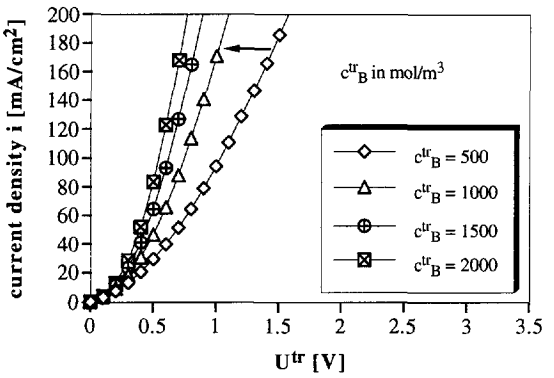

Fig. 29. Influence of c_B on the current–voltage curve.

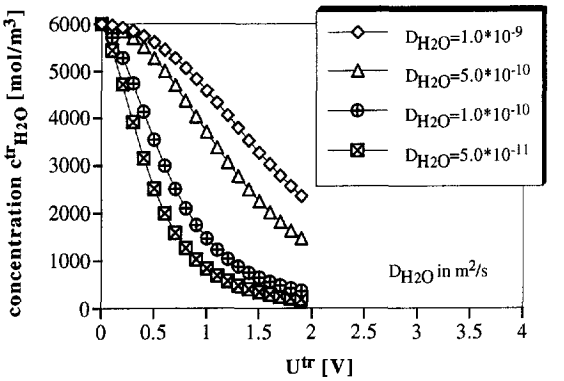

Fig. 31. Influence of D_{H_2O} on the water concentration in the transition region.

the basicity on the current–voltage curve. With increasing pK_b (decreasing basicity) the current density i at given voltage U^{tr} is increasing due to the increasing water dissociation. At $pK_b = 7$ the current density reaches its maximum value. With increasing concentration of basic groups c_B the current density is increasing as shown in Fig. 29.

By decreasing the diffusion coefficient of water in the membrane, the water flux into the transition zone decreases and thus its water concentration also decreases. As shown in Eqs. (56) and (57) the concentration of H_3O^+- and OH^--ions depends on the water concentration. If the water concentration is decreasing the proton and hydroxyl ion concentrations as well as the electric current as calculated from Eq. (61) are decreasing.

If the water concentration in the transition region reaches very small values, the water dissociation and

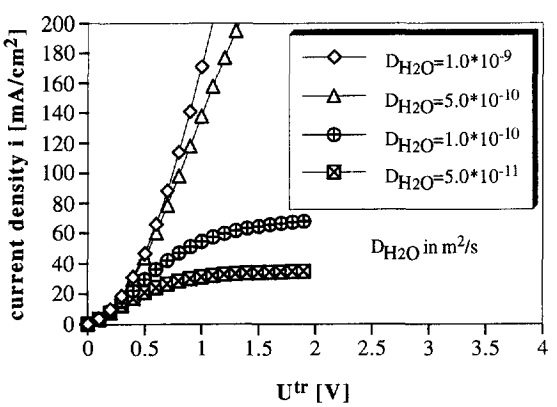

Fig. 30. Influence of D_{H_2O} on the current–voltage curve.

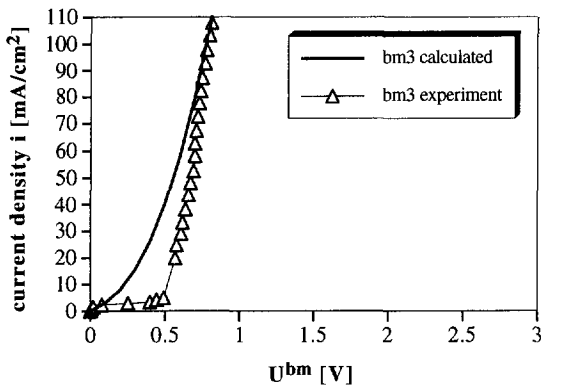

Fig. 32. Calculated and measured current–voltage curve for bipolar membrane bm3 (parameters used for the calculation: $pK_b = 5.9$, $D_{H_2O} = 10^{-8}$ m^2 s^{-1}, $c_B = 1000$ mol m^{-3}).

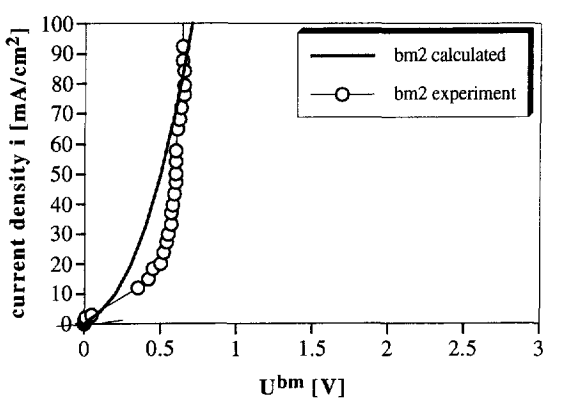

Fig. 33. Calculated and measured current–voltage curve of bipolar membrane bm2 (parameters used for the calculation: $pK_b = 6.0$, $D_{H_2O} = 10^{-8}$ m^2 s^{-1}, $c_B = 1000$ mol m^{-3}).

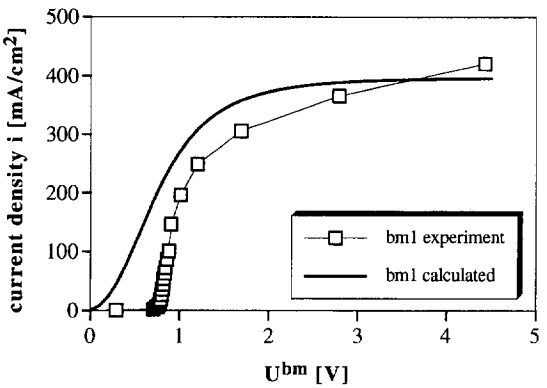

Fig. 34. Comparison between calculated and measured current–voltage curve for bipolar membrane bm1 showing the limitation of water diffusion into the membrane at high current density (parameters used for the calculation: $pK_b = 6.2$, $D_{H_2O} = 5.5 \times 10^{-10}$ m^2 s^{-1}, $c_B = 1500$ mol m^{-3}).

hence the current density is limited by the diffusion of water into the membrane. Figs. 30 and 31 show the influence of D_{H_2O} on the current density i and the water concentration $c^{tr}_{H_2O}$.

Calculated and measured current–voltage curves are shown in Figs. 32–34. In Figs. 32 and 33 it can be seen that by using realistic values for pK_b and c_B, the experimentally measured current densities agree well with data calculated with the suggested model. It should be noted that this model describes the electric current due to the water dissociation process (transport of protons and hydroxyl ions out of the transition region) and thus predicts the current–voltage behaviour of bipolar membranes at higher current densities quite well. Fig. 34 shows the measured and calculated limitation of the current density due to diffusion of water into the membrane bm1.

5. Conclusions

In this paper the properties of bipolar membranes are discussed. When a low electric field strength is applied, salt ions removed from the transition region of the bipolar membrane by migration are replaced by salt diffusing and migrating from the bulk solutions into the transition region resulting in a steady state with a constant salt concentration in the transition region. When the electric field is increased the migration from the transition region can no longer be compensated by the diffusive flux into the transition region which then becomes completely depleted of salt ions and a limiting current density is reached. The limiting current density depends on the permselectivity of the bipolar membrane as well as on the diffusion coefficient of the salt in the membrane. When the limiting current density is exceeded, water dissociation begins and the current is now carried by protons and hydroxyl ions.

The water dissociation can be described by a model which combines the calculation of the reaction zone thickness, the protonation and deprotonation of weakly basic or acidic groups and the influence of the electric field on the dissociation rate constants, i.e. the second Wien effect. The results indicate that the water splitting in bipolar membranes takes place in a very small region of the monopolar ion-exchange layer where uncompensated fixed charges exist as indicated in the schematic drawing of Fig. 35.

The protonation and deprotonation can take place at basic and at acidic groups. The pK_b or pK_a value of these groups has to be in a range between 4 and 10. The thickness of the transition region between the ion-exchange layers, which includes the reaction zone, is a few nanometers.

Due to the roughness of the polymer surfaces, in some cases there might be thin neutral regions (water layer) between the ion-exchange layers as illustrated in Fig. 36. The presence of these regions depends on the production of the bipolar membrane. In the case of the studied commercial bipolar membranes bm1,

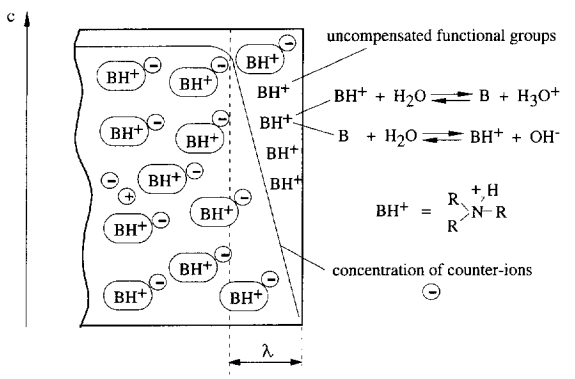

Fig. 35. Mechanism of water dissociation at uncompensated functional groups of the anion-exchange layer.

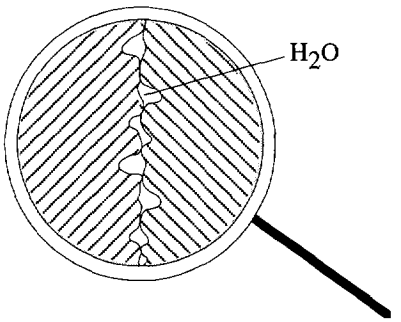

Fig. 36. Presence of a thin water layer between the monopolar membrane.

bm2, and bm3 the presence of a thin water layer can be excluded. However, uncertainty exists about the value of the relative permittivity ϵ_r in the reaction zone and the influence of the electric field on the rate constants k.

6. List of Symbols

6.1. Roman letter symbols

a	activity (mol m^{-3})
A	area (m^2)
c	concentration (mol m^{-3})
D	diffusion coefficient (m^2 s^{-1})
d	half distance between two membranes (m)
E	electric field strength (V m^{-1})
e_0	elementary charge, 1.602×10^{-19} (A s)
F	Faraday constant, 96486 (A s mol^{-1})
I	electric current (A)
i	current density (A m^{-2}), (mA cm^{-2})
J	flux (mol m^{-2} s^{-1})
K	equilibrium constant (mol l^{-1})
K_w	equilibrium constant of water, 10^{-14} (mol^2 l^{-2})
k	Boltzmann's constant 1.38×10^{-23} (kg m^2 s^{-2} K^{-1})
k	rate constant (m^3 mol^{-1} s^{-1}), (s^{-1})
N_A	Avogadro's number 6.023×10^{23} (molecules mol^{-1})
pK_a	$-\log K_a$
pK_b	$-\log K_b$
R	gas constant 8.314 (Nm mol^{-1} K^{-1})
r	reaction rate (mol m^{-3} s^{-1})
r_e	area-multiplied resistance (Ω cm^2)
T	temperature (K)
t	time (s)
t, t^*	transport number
U	potential difference (V)
u	mobility (cm^2 s^{-1} V^{-1})
X	fixed charge density (mol l^{-1}), (mol m^{-3})
z	electric valence

6.2. Greek Letter Symbols

ϵ_0	permittivity of free space, 8.85×10^{-12}(A s V^{-1} m^{-1})
ϵ_r	relative permittivity
κ	conductivity (A V^{-1} m^{-1})
2λ	thickness of the transition or neutral layer (m)
φ	electric potential (V)
ρ_e	space charge density (A s m^{-3})
ω	valence of the fixed charge
Δ	difference
δ_m	thickness of anion- or cation-exchange layer (m)

6.3. Superscripts

aem	anion-exchange membrane
cem	cation-exchange membrane
b	bulk solution
b_1	bulk solution at the cation-exchange side
b_2	bulk solution at the anion-exchange side
bm	bipolar membrane
m	membrane
tr	transition layer
mb	interphase membrane–bulk solution
mtr	interphase membrane–transition region
0	start value at time $t = 0$

6.4. Subscripts

j	species j
Don	Donnan
theo	theoretical value
a	acid
b	base

Acknowledgements

The authors gratefully acknowledge the financial support of the European Commission in the frame of the "Human Capital and Mobility Network-Functional Membranes".

References

[1] R. Schlögl and U. Schlödel, Über das Verhalten geladener Porenmembranen bei Stromdurchgang, Zeit. Phys. Chem., 5 (1955) 372–397.
[2] K.S. Spiegler, Transport processes in ionic membranes, Trans. Faraday Soc., 54 (1958) 1408–1428.
[3] F. Bergsma and Ch. A. Kruissink, Ion-exchange membranes, Fortschr. Hochpolym.-Forsch., Bd. 2 (1961) 307–362.
[4] R. Schlögl, Stofftransport durch Membranen, Dr. Dietrich Steinkopff Verlag, Darmstadt, 1964.
[5] W.H. Koh and H.P. Silverman, Anion transport in thin-channel cation exchange membranes, J. Membrane Sci., 13 (1983) 279–290.
[6] Mitsuro Higa, Akihiko Tanioka and Keizo Miyasaka, Simulation of the transport of ions against their concentration gradient across charged membranes, J. Membrane Sci., 37 (1988) 251–266.
[7] M.W. Verbrugge and P.N. Pinatauro, Transport model for ion-exchange membranes, in B.E. Conway, J.O'M. Bockris and R.E. White (Eds.), Modern Aspects of Electrochemistry, 19, Plenum, 1989.
[8] Mitsuro Higa, Akihiko Tanioka and Keizo Miyasaka, A study of ion permeation across a charged membrane in multicomponent ion systems as a function of membrane charge density, J. Membrane Sci., 49 (1990) 145–169.
[9] V.I. Zabolotsky and V. Nikonenko, Effect of structural membrane inhomogeneity on transport properties, J. Membrane Sci., 79 (1993) 181–198.
[10] F.-F. Kuppinger, W. Neubrand, H.-J. Rapp and G. Eigenberger, Electromembrane processes Fundamentals and mathematical modelling, Chem. Ing. Techn., 67(4) (1995) 441–448.
[11] F.-F. Kuppinger, W. Neubrand, H.-J. Rapp and G. Eigenberger, Electromembrane processes – Part 2: Applications, Chem. Ing. Techn., 67 (1995) 731–739.
[12] K. Nagasubramanian, F.P. Chlanda and K.-J. Liu, Use of bipolar membranes for generation of acid and base – An engineering and economic analysis, J. Membrane Sci., 2 (1977) 109–124.
[13] K.N. Mani, F.P. Chlanda and C.H. Byszewski, Aquatech membrane technology for recovery of acid/base values from salt streams, Desalination, 68 (1988) 149–166.
[14] H.J. Rapp, Elektrodialyse mit bipolaren Membranen – Theorie und Anwendung, Ph.D Thesis, Universität Stuttgart, Institut für Chemische Verfahrenstechnik, 1995.
[15] N.-T. Dang and D. Woermann, Efficiency of the generation of protons and hydroxyl ions in bipolar membranes by electric field enhanced water dissociation, Ber. Bunsenges. Phys. Chem., 97 (1993) 149–154.
[16] A. Mauro, Space charge regions in fixed charge membranes and the associated property of capacitance, Biophys. J., 2 (1962) 179–198.
[17] R. Simons, The steady and non-steady state properties of bipolar membranes, Biochim. Biophys. Acta, 274 (1972) 1–14.
[18] H.G.L. Coster, A quantitative analysis of the voltage–current relationships of fixed charge membranes and the associated property of "punch-through", Biophys. J., 5 (1965) 669–686.
[19] R. Simons and G. Khanarian, Water dissociation in bipolar membranes: Experiments and theory, J. Membrane Biol., 38 (1978) 11–30.
[20] F. Maletzki, H.-W. Rösler and E. Staude, Ion transfer across electrodialysis membranes in the overlimiting current range, J. Membrane Sci., 71 (1992) 105–115.
[21] T.-C. Huang and I.-Y. Yu, Correlation of ionic transfer rate in electrodialysis under limiting current density conditions, J. Membrane Sci., 35 (1988) 193–206.
[22] H. Strathmann, H.-J. Rapp, B. Bauer and C.M. Bell, Theoretical and practical aspects of preparing bipolar membranes, Desalination, 90 (1993), 303–323.
[23] F. Helferich, Ionenaustauscher – Band 1 Grundlagen, Verlag Chemie GmbH, Weinheim, 1959.
[24] I. Rubinstein, A. Warshawsky, L. Schechtman and O. Kedem, Elimination of acid–base generation ("water-splitting") in electrodialysis, Desalination, 51 (1984) 55–60.
[25] R. Simons, The origin and elimination of water splitting in ion exchange membranes during water demineralisation by electrodialysis, Desalination, 28 (1979) 41–42.
[26] R. Simons, Electric field effects on proton transfer between ionizable groups and water in ion exchange membranes, Electrochim. Acta, 29 (1984) 151–158.
[27] R. Simons, Water splitting in ion exchange membranes, Electrochim. Acta, 30(3) (1985) 275–282.
[28] L. Onsager, Deviations from Ohm's law in weak electrolytes, J. Chem. Phys., 2 (1934) 599–615.
[29] B. Bauer, F.J. Gerner and H. Strathmann, Development of bipolar membranes, Desalination, 68 (1988) 279–292.
[30] P.W. Atkins, Physical Chemistry, 5th edn., Oxford University Press, Oxford, UK, 1994.